JOURNAL OF MATERIALS SCIENCE 24 (1989) 1693–1699

Influence of nitrogen ion implantation on hydrogen permeation in an extra mild steel

A. M. BRASS*, J. CHENE*, J. C. PIVIN†
*CNRS UA 1107, Laboratoire de Métallurgie Structurale, U.P.S. Orsay Cedex, 91405, France
†C.S.N.S.M. BP 1 – Orsay, France

This paper presents the first results on the effect of nitrogen implantation on hydrogen permeation in steels. Nitrogen can modify superficially the steel's chemistry and/or microstructure depending on the fluence and thereby affect the processes of hydrogen diffusion and trapping. The implantations were performed on low carbon steel specimens with different nominal doses (1% to 10% and 33% nitrogen in a superficial layer of approximately 100 to 120 nm). The corresponding microstructures were characterized and permeation tests were conducted at room temperature in a double electrolytic cell. The nitrogen implanted layers on iron affects the electrochemical behaviour of the surface and the permeation in the material. This effect depends on the nitrogen concentration in the layer and on the corresponding microstructure. A continuous Fe_2N layer acts as an efficient barrier to hydrogen entry and permeation when the layer is located on the entry face of the permeation membrane. This effect is stronger when the implanted layer is on the downstream face of the membrane. The low permeability values are mainly attributed to a lower hydrogen solubility in the implanted layer, whereas hydrogen trapping on defects and nitride precipitates delay hydrogen penetration.

1. Introduction

Many studies have been devoted to steels implanted with nitrogen ions because of the improvement of wear [1, 2] and corrosion resistance [3, 4] provided by this surface treatment. Since hydrogen embrittlement and stress corrosion cracking are a major problem in engineering materials [5], it is important to have a better insight in the processes of hydrogen diffusion and trapping, including the preliminary step of (ad) absorption. Hydrogen (or deuterium) diffusion and trapping in iron and steels have been investigated on basis of concentration profiles in samples implanted with hydrogen or deuterium [6, 7] or in electrolytically hydrogenated specimens [8]. Work is still in progress in order to try to reduce the hydrogen entry in the metal and to design steels microstructure such that the microstructural trapping sites play a beneficial role [9, 10] when hydrogen penetration cannot be avoided (for given environment and mechanical solicitations). A few studies of hydrogen permeation in iron membranes implanted with platinum, iron, helium [11] and cerium [12] are reported in the literature. This paper presents the first results on the effect of nitrogen implantation on hydrogen permeation in steels. Nitrogen was chosen because this element can modify superficially the steel's chemistry and/or microstructure depending on the fluence. Nitrogen implantation is also currently used as an industrial surface treatment.

The results described here address the following questions.

(i) To what extent implanted nitrogen reduces cathodic hydrogen permeation through a low carbon steel?

(ii) What is the effect of the nitrogen content in the implanted layer on hydrogen permeation?

(iii) Does the hydrogen permeability depend on the location of the implanted layer on the permeation membrane?

2. Experimental procedure

A low carbon steel (1 mm thick sheet as-received) was used to prepare samples for ion implantations and hydrogen permeation tests. Its chemical composition and thermal treatments are given in Table I.

The unimplanted material exhibited a ferritic structure (grain size $\simeq 30\,\mu m$) with a small amount of globular perlite. After mechanical polishing down to a $1\,\mu m$ diamond paste (average roughness $0.02\,\mu m$), the samples were implanted in the C.S.N.S.M. machine [13] under a vacuum better than 10^{-7} torr (temperature $\simeq 20°C$).

The implantations were performed successively with ions of different energies in order to obtain a flat profile. The chosen energies of 80, 40 and 15 keV and the ratio of fluences of 1.066 and 0.33 were determined on the basis of TRIM simulations [14]. The microstructures obtained were observed by optical microscopy and by TEM after thinning the specimens from the unimplanted side (double jet electropolishing at

TABLE I Chemical composition and heat treatment of the low carbon steel

	Cr	Ni	Mo	Mn	C	P	Si	S	Al	Cu
	(wt %)				(p.p.m. wt)					
Low carbon steel	0.029	0.027	–	.20	530	110	110	80	450	140
	heat treatment 920° C 1 h A.Q. + 24 h 700° C									

0022–2461/89 $03.00 + .12

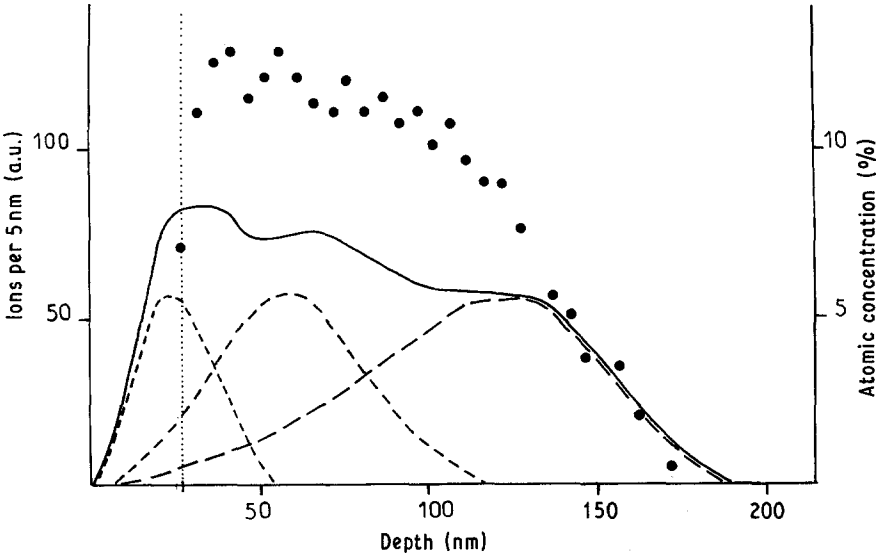

Figure 1 Computer simulation of the distribution of implanted ions for 1000 incident ions of 80 keV (——) +660 of 40 keV (——) +330 of 15 keV (--) and sum profile (continuous lines). Experimental distribution (●) in a sample implanted with a nominal fluence of 1.8×10^{17} N (10% N) deduced from the RBS profile of iron atoms. It has been shifted of 27 nm (broken curve), the depth of which is an overestimation of the sputtered thickness (on the basis of the sputtering yield measured by Barnavon [22] for the intermediate energy of 40 keV).

50 V in a mixture of ethanol 60% vol, butanol 35% vol and perchloric 5% vol, thermostatted at −25° C; the implanted side of the specimens was protected by a translucent varnish coating).

Permeation tests were made in a double electrolytic cell [15] thermostatted at 25 ± 0.5° C. In this method, the membranes are cathodically charged with hydrogen in a 0.1 N NaOH solution on one side while on the other side, the hydrogen which has diffused through the membrane is anodically oxidized in a 0.1 N NaOH solution.

The permeation data are obtained as follows:

(i) Deaeration of the solutions by bubbling argon and measurement of the dissolution potential E_d on the exit side until it reaches a constant value.

(ii) Recording of the residual current density i while the exit surface is polarized at the E_D potential value (i is typically less than 20 nA cm^{-2}).

(iii) Introduction of the deaerated NaOH solution in the charging chamber of the cell and potentiostatic polarization of the entry face of the sample at −1.35 V/SCE (cathodic charging conditions).

The recorded anodic current is a direct measurement of the hydrogen flow through the membrane. When a stationary permeation current is established, the cathodic polarization is stopped and the decrease of the hydrogen flux is recorded on the exit face of the specimen while the entry side is passivated at 0 V/SCE.

Potentiostatic polarization curves have also been recorded in 0.1 N NaOH in order to detect a possible change in the electrochemical behaviour of the implanted surface as a function of the nitrogen concentration.

3. Results

3.1. Nitrogen profiles

The theoretical distribution of implanted atoms is nearly Gaussian but films with a homogeneous composition over several hundreds of nanometres can be obtained by combining implantation at several energies. However the predicted distribution is only valid for low implanted fluence (as the composition and density of the targets remain constant) and the effects of radiation induced diffusion and of phase transformations are not taken into account. The result of TRIM calculations is plotted on Fig. 1 together with the experimental profile recorded by Rutherford backscattering spectrometry (RBS) on a sample implanted with 10% nitrogen. The numbers of nitrogen, carbon and oxygen atoms dosed by NRA in the unimplanted steel and in samples implanted with 10%, 33% nitrogen are reported in Table II.

These results show that the nitrogen implanted layer is approximately 100 to 120 nm thick for a fluence of 2×10^{17} atoms cm^{-2}. The accuracy of the depth scale of RBS profile is of the order of 10% and the depth resolution of 10 nm. The depth profile (determined by SIMS for all concentrations and RBS for 33% nitrogen) and the amount of contamination were sensibly the same for all concentrations. Table II shows that the carbon and oxygen contamination during implantation is extremely low. The nitrogen amount measured in the unimplanted specimen is the bulk content on several micrometres (as attested by the energy width of the NRA peak) and it corresponds to a concentration lower than 0.1%.

3.2. Compounds formed during implantation

The formation of small sized precipitates, high densities of dislocations and martensitic transformations induced by nitrogen implantation in iron and steels are responsible for the hardening of implanted layers. Even pure iron changes into α' nitrogen martensite for a concentration of implanted nitrogen as low as 1% [17]. When the nitrogen dose is increased, the iron

TABLE II NRA and RBS results on unimplanted, 10% and 33% nitrogen implanted steel

Specimen	Nominal dose ($\times 10^{15}$ cm^{-2})	Atoms dosed ($\times 10^{15}$ cm^{-2})			Film thickness (nm)*
		N	O	C	
Unimplanted steel	0	20	30	15	
Fe–10% N film	165	200	30	20	120
Fe–33% N film	400	365	40	20	100

*Deduced from the total amounts of nitrogen and iron measured respectively by NRA and RBS and of the known density for the measured N/Fe stoichiometry ratio.

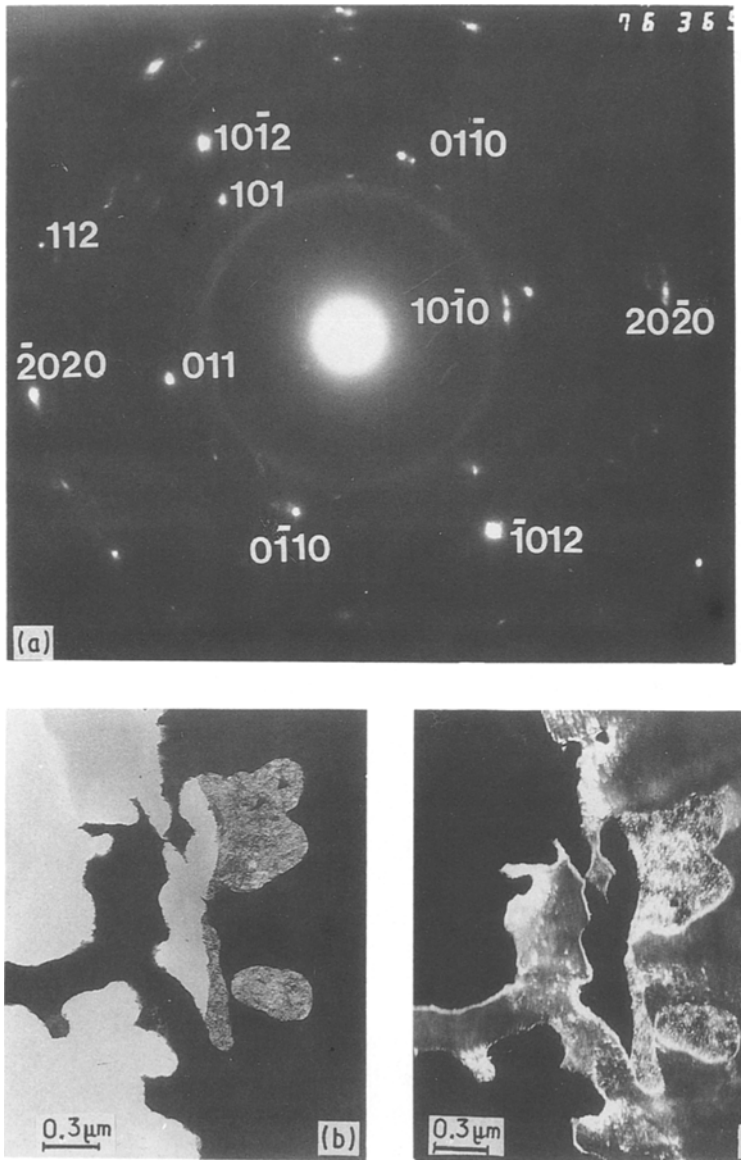

Figure 2 TEM observations on a low carbon steel implanted with 33% nitrogen. (a) Bright field image of 33% nitrogen implanted steel. (b) Dark field image of diffracting Fe_2N grains. (c) Corresponding diffractogram.

nitride ε-Fe_2N precipitates, forming a continuous layer in samples implanted with 33% nitrogen. The layer containing 10% nitrogen is constituted by a mixture of the α' and ε-Fe_2N phases [17, 18].

TEM observations have been performed on a sample implanted with 33% nitrogen (Fig. 2a). The implantation layer was single phased and constituted of fine grains of the hexagonal Fe_2N phase, as expected for this concentration. These grains exhibited preferential orientation relationships within blocks (see dark field image and diffractogram on Figs 2b and c) because they have grown in epitaxy with the iron lattice. However they presented several epitaxial relationships with iron:

$\{0\,0\,0\,1\} \parallel \{1\,1\,0\}$ Fe with $\langle 1\,1\,\bar{2}\,0\rangle \parallel \langle 1\,1\,0\rangle$ Fe (this epitaxial relationship has previously been reported [17, 18].

$\{1\,0\,\bar{1}\,0\} \parallel \{1\,0\,0\}$ or $\{1\,1\,0\}$ Fe with $\langle 1\,1\,\bar{2}\,0\rangle \parallel \langle 1\,1\,0\rangle$ Fe

The distances between iron in these directions are comparable: 0.277 nm along $\langle 1\,1\,\bar{2}\,0\rangle$ in the nitride against 0.287 nm along $\langle 1\,0\,0\rangle$ in iron. However the precipitates do not collapse in a single mosaic crystal of Fe_2N within each iron grain since several blocks with different epitaxies can develop and part of them are randomly oriented (rings on Fig. 2c).

3.3. Electrochemical behaviour of implanted surfaces

Potentiostatic cathodic polarization curves of surfaces implanted with nitrogen in deaerated 0.1 N NaOH are shown in Fig. 3. Only slight changes can be observed between the implanted and unimplanted specimens: the corrosion potential of implanted surfaces is a little more noble, the hydrogen exchange current density slightly higher and the hydrogen overvoltage lower. Such electrochemical behaviour will tend to reduce the hydrogen entry in implanted specimens. However the effect of nitrogen implantation on the kinetic of hydrogen discharge in NaOH is less pronounced than the observed effect with other implanted species [11]. Then the catalytic effect of nitrogen is not expected to play a major role on hydrogen entry and permeation for the selected charging conditions.

Metallographic observations after chemical attacks in Nital clearly show large differences in the microstructure and the chemical reactivity of the surface as a function of the nitrogen concentration.

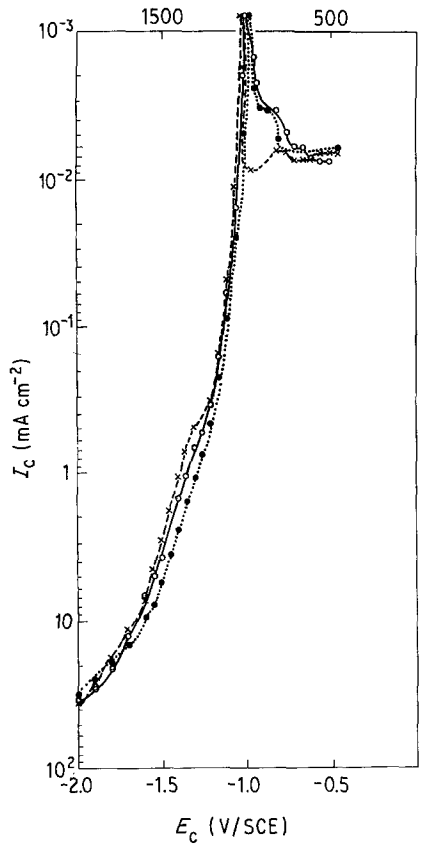

Figure 3 Potentiostatic cathodic polarization curves as a function of nitrogen concentration implanted in low carbon steel (0.1 N NaOH) (× 0% $I_0 = 3.2 \times 10^{-5}$ A cm^2, ● 1% $I_0 = 1.5 \times 10^{-5}$ A cm^2, ○ 33% $I_0 = 4.6 \times 10^{-5}$ A cm^2).

Fig. 4a illustrates this difference for a surface implanted with 33% nitrogen and an unimplanted one, indicating a large beneficial effect of nitrogen on the corrosion resistance. A prolonged etching of the surface implanted with 33% nitrogen leads to a preferential attack of the globular perlite precipitates (Fig. 4b) in a reverse manner of what has been observed for lower nitrogen concentration (Fig. 4c). This fact indicates that the Fe_2N film built on the ferritic matrix is more noble than the unidentified Fe–N–C compound formed upon cementite precipitates (initially less reactive than ferrite).

3.4. Permeation and degassing measurements

A special attention has been paid to the role of the position of the implanted layer in the permeation cell.

3.4.1. Implanted layer on the entry side of the permeation membrane

Permeation and desorption rates as a function of nitrogen content are plotted on Figs 5 and 6. The main diffusion data computed from these curves are reported in Table III.

b.t. is the break-through time and d.t. the delay time at the beginning of the degassing step. Among the various methods available for D_{app} (apparent diffusion coefficient) calculation [19] the time lag (t.l.) and the break-through time (b.t.) or delay time for degassing (d.t.) methods were chosen. The use of d.t. which is considered to be the less affected by the deep trapping (if any), leads always to the largest D_{app} values, the more representative of the diffusion of lattice and weakly trapped hydrogen.

An implantation of 33% nitrogen reduces drastically the hydrogen permeability (P). D_{app} is in this case diminished by a factor of 10 to 20 and the b.t. is approximately 14 times longer. Hydrogen diffusivity through steels implanted with 1% and 10% N is only slightly slower than in the "reference steel".

The degassing curves show a fairly rapid hydrogen desorption from the unimplanted steel. The hydrogen release is greatly delayed by an implantation of 33% nitrogen: d.t. is increased by a factor of 20 as compared to the unimplanted material.

Concerning the 1% and 10% nitrogen implanted steels the latter releases hydrogen faster than the former. Hydrogen degassing is slower in both cases as compared to the reference.

3.4.2. Implanted layer on the exit side of the permeation membrane

Permeation curves are plotted on Fig. 7 for the samples implanted with 10% and 33% nitrogen, together with the permeation data of Fig. 5 replotted on Fig. 7 in dashed lines. In the case of the sample implanted with 33% nitrogen no hydrogen permeation could be detected after 4 days with a polarization at −1.35 V/SCE. Then, the hydrogen fugacity on the input (unimplanted) face of the membrane was increased by changing the applied potential to a more cathodic value (−2.5 V/SCE). The corresponding diffusion data are reported in Table IV.

For both 10% and 33% nitrogen concentrations the hydrogen permeability is decreased by a factor of 10 to more than 40 as compared to the reference, when the

TABLE III Permeation and desorption data as a function of nitrogen content when implanted layers are on the entry side of the permeation membrane

	Unimplanted steel	1% N implanted steel	10% N implanted steel	33% N implanted steel
b.t. (1st transient) (sec cm)	15	20	40	320
d.t. (degassing) (sec cm)	1	25	3	60
P (cm^3 cm cm^{-2} sec^{-1})	8.2×10^{-9}	1.1×10^{-8}	6.8×10^{-9}	3×10^{-9}
D_{app} (b.t.) (cm^2 sec^{-1})	2×10^{-6}	1.8×10^{-6}	1×10^{-6}	2×10^{-7}
D_{app} (t.l.) (cm^2 sec^{-1})	3.3×10^{-7}	4.7×10^{-7}	2.1×10^{-7}	4.5×10^{-8}
D_{app} (d.t.) (cm^2 sec^{-1})	3×10^{-5}	1.3×10^{-6}	1.2×10^{-5}	5.5×10^{-7}
Q_{diff} (cm^3 cm^{-3})	3.7×10^{-7}	1×10^{-2}	1.8×10^{-3}	7×10^{-3}
C_0 (d.t.) (cm^3 cm^{-3})	2.7×10^{-4}	8.5×10^{-3}	5.7×10^{-4}	5.4×10^{-3}

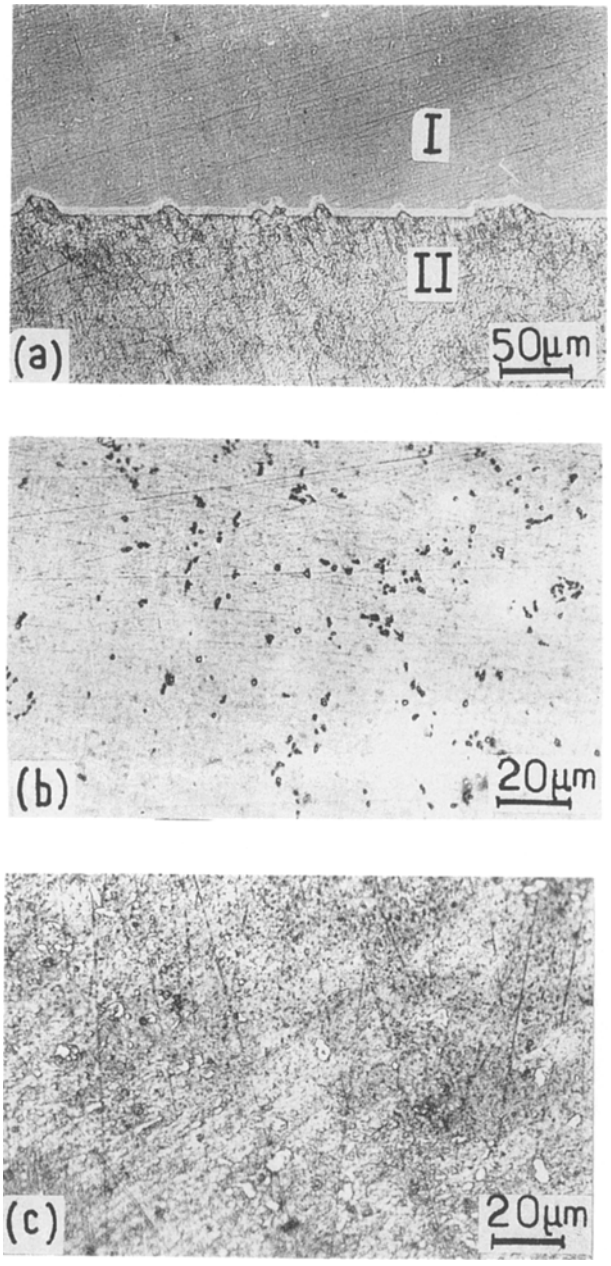

Figure 4 Microstructure of a low carbon steel implanted with nitrogen. (a) (I) zone implanted with 33% N, (II) unimplanted zone. (b) surface implanted with 33% N after severe attack. (c) surface implanted with 10% N.

implanted layer is located on the downstream face of the membrane. In this situation b.t. and D_{app} (d.t.) are not significantly modified and the kinetic of hydrogen release is only slightly slower than in the case of unimplanted samples. D_{app} (t.l.) value is even found larger for the 10% nitrogen implanted steel.

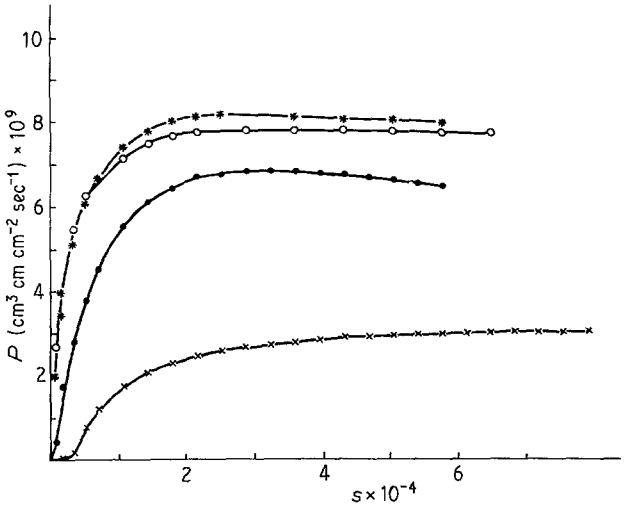

Figure 5 Permeation curves for 1% N (○), 10% N (●) and 33% N (×) implanted low carbon steel (implanted layer on the entry side of the permeation membrane) (*unimplanted steel).

5. Discussion

Diffusion coefficient through the implanted layers can be deduced from the degassing data when the implanted side of the membranes faces the detection part of the permeation cell. One of the first conclusions is that the hydrogen diffusivity is not significantly smaller in the implanted material whatever the nitrogen concentration as compared to the reference steel. Furthermore no concentration dependency for D_{app} is evident in the implanted layer (see D_{app} (d.t.) values of Table IV).

The *decrease of all* D_{app} values when hydrogen is electrolytically produced on the implanted layer may be attributed to trapping in this layer and (or) to a smaller hydrogen concentration in the implanted part of the membrane as compared to the equilibrium concentration in the ferritic structure. The latter effect would then imply a concentration dependency of D_{app}.

If the hydrogen diffusion is considered to be independent of any concentration gradient, the decrease of D_{app} (b.t.) and D_{app} (t.l.) together with the increase of b.t. values whatever the location of the implanted face can be attributed to trapping in (or underneath) the implanted layer. This effect is particularly strong for steel implanted with 33% nitrogen covered by a continuous film of iron nitrides (and dislocations). D_{app}

TABLE IV Permeation and desorption data for 10% and 33% nitrogen concentration when implanted layers are on the exit side of the permeation membrane

	Unimplanted steel	10% N steel	33% N steel
b.t. (1st transient) (sec cm)	15	30	$> 3 \times 10^5$ (12)
d.t. (degassing) (sec cm)	1	3	(6)
P (cm^3 cm cm^{-2} sec^{-1})	8.2×10^{-9}	7.8×10^{-10}	0 after 4 days (1.9×10^{-10})
D_{app} (b.t.) (cm^2 sec^{-1})	2×10^{-6}	1.4×10^{-6}	
D_{app} (t.l.) (cm^2 sec^{-1})	3.3×10^{-7}	1.3×10^{-6}	(1.6×10^{-9})
D_{app} (d.t.) (cm^2 sec^{-1})	3×10^{-5}	1.2×10^{-5}	1×10^{-5}

The values in brackets correspond to the following charging conditions: −2.5 V/SCE applied after a 4 days polarization at −1.35 V/SCE.

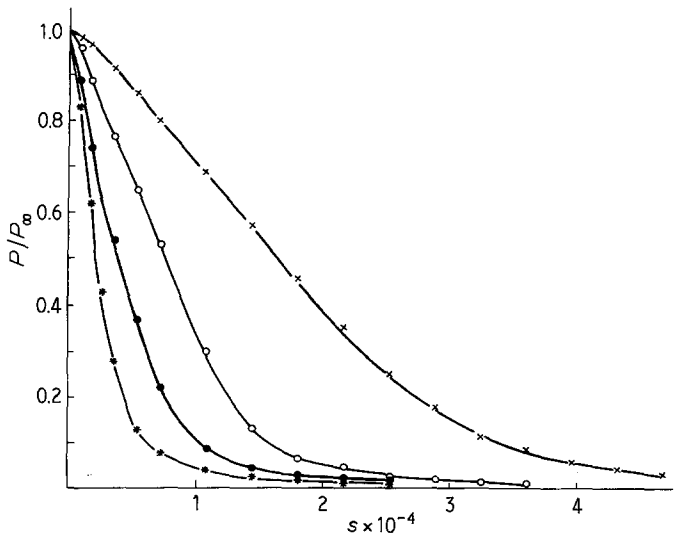

Figure 6 Desorption rate as a function of implanted nitrogen concentration in a low carbon steel (implanted layer on the entry side of the permeation membrane). (*unimplanted steel, o 1% N implanted steel, • 10% N implanted steel, x 33% N implanted steel)

(t.l.) include the contribution of the "deepest" traps available in the material if any; its value is much smaller for the 33% nitrogen steel. This tends to show that the iron nitrides act as relatively high energy traps.

The 1% nitrogen layer contains a very high density of dislocations which are responsible for the increase of b.t. and d.t. values (Table III) and the decrease of D_{app} (d.t.) value.

Whereas the interaction energy of dislocations with hydrogen is known to be small in the ferritic structures, the trapping energy of iron nitrides is not reported in the literature. The comparison of the results obtained for the 1% and 33% nitrogen implanted samples indicates that iron nitrides are more effective traps than dislocations.

The *low permeability values* measured on the 10% and 33% specimens can be attributed to differences in the hydrogen entry mechanism on the implanted face or to a smaller hydrogen solubility in the implanted layer when compared to the unimplanted material. The role of nitrogen concentration on the electrochemical behaviour rules out a major catalytic effect of the implanted specie. Only a smaller hydrogen solubility in the implanted layer can explain the large permeability drop. This drop is more pronounced when the implanted side of the membrane faces the detection part of the cell because in this case, the concentration gradient in the layer is even smaller. This behaviour is in agreement with a previous extensive work on concentration effects on hydrogen permeability in superficially oxidized steels [20].

It is interesting to note that the *hydrogen desorption kinetic* recorded on the unimplanted face of the membrane (Table III and Fig. 6) is markedly influenced by the presence of an implanted layer on the entry face of the specimen. As reversible trapping process may slow down the desorption, this effect together with a smaller hydrogen solubility in the implanted layer can account for the slow desorption rate observed for the steels implanted with 1% and 33% nitrogen.

Hydrogen degassing through the implanted layer (when it is located on the down stream side of the specimen) is not significantly delayed because in this situation, the desorption through the entry face is not disturbed (unimplanted metal). The delay time of degassing depends partly on the diffusion characteristics of hydrogen in microstructure on the exit side of the specimen and also on the relative variation as a function of time of the concentration gradients in the two different parts of the sample (implanted and unimplanted metal).

As the concentration gradient in the implanted layer is smaller when it is located on the exit side of the membrane the d.t. value is smaller when compared to the other situation.

By integrating the degassing curves, reversibly trapped hydrogen quantities can be theoretically estimated if the hydrogen lattice concentration is known. Hydrogen solubility may vary from one implanted specimen to the other depending on the chemical composition of the layer in contact with the electrolyte. Nevertheless our data show that the *total diffusible hydrogen concentration* Q_{diff} (see Table III) is larger for the 1% and 33% nitrogen implanted steel as compared to the reference. According to Fick's laws only one third of diffusible hydrogen can desorb through the downstream face of a homogeneous permeation membrane for the boundary conditions fixed in our

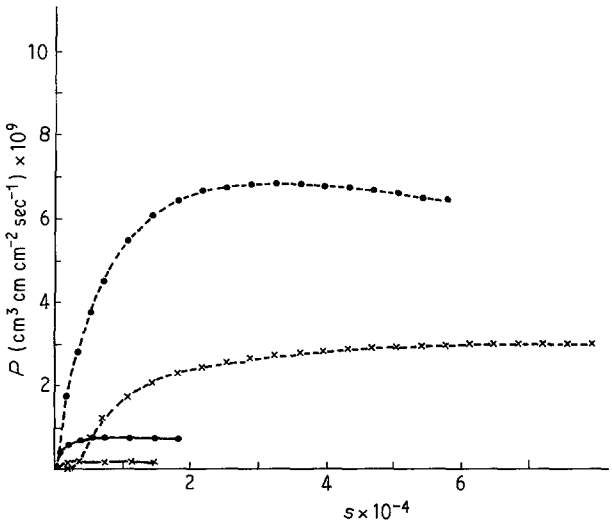

Figure 7 Permeation curves for 10% and 33% N concentration when the implanted layer is on the exit side of the permeation membrane. Broken curves correspond to the curves of Fig. 3.

experimental procedure [21]. However, if hydrogen solubility in the implanted layer is smaller than the solubility in the steel, more than one third of the diffusible hydrogen quantity present in the membrane when the polarization is interrupted will diffuse through the exit side, as the concentration gradient and D_{app} are larger in the unimplanted metal. This can explain the variation of Q_{diff} as a function of nitrogen concentration.

The steel implanted with 10% nitrogen exhibits contradictory behaviour: the implanted layer acts as a "barrier" during the first polarization transient but the degassing rate is faster when compared to the 1% nitrogen implanted steel. This result might be due to the presence of various phases in the 10% nitrogen implanted layer; its explanation requires a more detailed knowledge of the microstructure of these phases.

6. Conclusions

The conclusions are as follows.

120 nm thick nitrogen implantation layers on iron strongly affect the electrochemical behaviour of the surface and the permeation in the material.

This effect depends on the nitrogen concentration in the layer and on the corresponding microstructure.

A continuous Fe_2N layer acts as an efficient barrier to hydrogen entry and permeation when the layer is located on the entry face of the permeation membrane. This effect is stronger when the implanted layer is on the downstream face of the membrane.

The low permeability values are mainly attributed to a lower hydrogen solubility in the implanted layer, whereas hydrogen trapping on defects and nitride precipitates delay hydrogen penetration.

References

1. H. HERMAN, *Nucl. Instrum. Meth.* **182–183** (1983) 887.
2. J. C. PIVIN, N.A.T.O., Advanced Study Institute "Materials modification by High-Fluence Ion Beams", Vianado Castelo, Sept. 1987, Nato Pub.
3. V. ASHWORTH, W. A. GRANT, R. P. M. PROCTER and E. J. WRIGHT, *Corros. Sci.* **18** (1978) 681.
4. P. ZHOU, X. LIU, Z. WANG, W. TIAN and S. ZHOU, *Nucl. Instrum. Met.* **B7/8** (1985) 195.
5. C. G. INTERRANTE and G. M. PRESSOUYRE (Eds.), Current Solutions to hydrogen problems in steels, A.S.M. 1982.
6. S. M. MYERS and W. R. WAMPLER, *Mater. Sci. Eng.* **69** (1985) 397.
7. B. M. U. SCHERZER, P. BORGESEN and W. MÖLLER, *Nucl. Instrum. Meth. Phys. Res.* **B15** (1986) 375.
8. G. FRECH and G. K. WOLF, *ibid.* **B15** (1986) 520.
9. J. C. CHARBONNIER, H. MARGOT-MARETTE, A. M. BRASS and M. AUCOUTURIER, *Met. Trans.* **16A** (1985) 935.
10. G. M. PRESSOUYRE, *ibid.* **9A** (1978) 1571.
11. M. ZAMANZADEH, A. ALLAM and H. W. PICKERING, *J. Electrochem. Soc.* **127** (1980) 1688.
12. G. FRECH, G. REISS and G. K. WOLF, *Mater. Sci. Engng* **69** (1985) 419.
13. J. CHAUMONT, F. LALU, M. SALOME, A. M. LAMOISE and H. BERNAS, *Nucl. Instrum. Meth.* **189** (1981) 193.
14. J. P. BIERSACK and L. G. HAZMARK, *ibid.* **174** (1980) 257.
15. M. A. V. DEVANATHAN and Z. STACHURSKI, *J. Electrochem. Soc.* **111** (1964) 619.
16. J. C. PIVIN, *Surf. Interf. Anal.* (1987) submitted.
17. S. FAYEULLE, Thèse Doctorat Etat. Université C. Bernard, Lyon I, France (1987).
18. B. RAUSHENBACH and A. KOLITSCH, *Phys. Status Solidi* **A80** (1983) 211.
19. A. M. BRASS, Thèse Doctorat ès Sciences, Orsay, France (1983).
20. P. TISON, Rapport CEA-R-5240, Service de documentation. CEN Saclay – 91191 Gif sur Yvette – cedex France.
21. L. NANIS and T. K. G. NAMBOODHIRI, *J. Electrochem. Soc.* **119** (1972) 691.
22. T. BARNAVON, Thèse docteur 3ème cycle Lyon (1982).

Received 9 May
and accepted 12 September 1988